Pitch-angle scattering of inner magnetospheric electrons caused by ECH waves obtained with the Arase satellite

M. Fukizawa[1*], T. Sakanoi[1], Y. Miyoshi[2], Y. Kazama[3], Y. Katoh[1], Y. Kasahara[4], S. Matsuda[5], A. Matsuoka[5], S. Kurita[6], M. Shoji[2], M. Teramoto[7], S. Imajo[2], I. Sinohara[5], S-Y. Wang[3], S. W-Y. Tam[8], T.-F. Chang[8], B.-J. Wang[3], C.-W. Jun[2]

[1] Graduate School of Science, Tohoku University, Sendai, Japan

[2] Institute for Space-Earth Environmental Research, Nagoya University, Nagoya, Japan

[3] Academia Sinica, Institute of Astronomy and Astrophysics, Taipei, Taiwan

[4] Graduate School of Natural Science and Technology, Kanazawa University, Kanazawa, Japan

[5] Institute of Space and Astronautical Science, Japan Aerospace Exploration Agency, Sagamihara, Japan

[6] Research Institute for Sustainable Humanosphere, Kyoto University, Uji, Japan

[7] Department of Space Systems Engineering, Faculty of Engineering, Kyushu Institute of Technology, Kitakyushu, Japan

[8] Institute of Space and Plasma Sciences, National Cheng Kung University, Tainan, Taiwan

Corresponding author: Mizuki Fukizawa (fukizawa.m@pparc.gp.tohoku.ac.jp)

Key Points:

- We found an event that electron cyclotron harmonic wave intensity correlated with electron flux in a loss cone with ~5 keV energy.
- The pitch-angle diffusion coefficient of 5 keV is larger than those of other energies when the electron temperature is 8 eV and the wave normal angle is 88.5°.
- The electron flux correlated with the ECH wave intensity can cause 557.7 nm auroral emission with ~200 R intensity.

Abstract

Electrostatic electron cyclotron harmonic (ECH) waves are generally excited in the magnetic equator region, in the midnight and the morning sectors during geomagnetically active conditions, and cause the pitch angle scattering by cyclotron resonance. The scattered electrons precipitate into the Earth's atmosphere and cause auroral emission. However, there is no observational evidence that ECH waves actually scatter electrons into the loss cone in the magnetosphere. In this study, from simultaneous wave and particle observation data obtained by the Arase satellite equipped with a high-pitch angular resolution electron analyzer, we present evidence that the ECH wave intensity near the magnetic equator is correlated with an electron flux inside the loss cone with energy of about 5 keV. The simulation suggests that this electron flux contributes to auroral emission at 557.7 nm with intensity of about 200 R.

Plain Language Summary

Wave-particle interaction via electrostatic electron cyclotron harmonic (ECH) waves is a promising generation mechanism for precipitating electrons into Earth's atmosphere and producing diffuse auroras. However, there is no observational evidence that ECH waves scatter electrons to cause auroral emissions. In this study, based on observation data obtained by the Arase satellite equipped with a high-angular resolution electron analyzer, we identified an event, during which the ECH wave intensity near the magnetic equator was correlated with the electron flux that precipitated into the Earth's atmosphere. Our simulation suggests that this electron flux contributes to visible oxygen green-line auroral emission.

1 Introduction

In the magnetospheric equator region of the Earth, various plasma waves are excited by injected plasma sheet particles. Electrostatic electron cyclotron harmonic (ECH) waves play a role in the generation of pulsating auroral emissions mainly in the morning (Fukizawa et al., 2018; Liang et al., 2010; Lyons, 1974), besides lower-band chorus (LBC) waves (Hosokawa et al., 2020; S. Kasahara et al., 2018; Miyoshi, Saito, et al., 2015).

ECH waves are electrostatic emissions excited in frequency bands between a multiple of the electron cyclotron frequency f_{ce}, and they are sometimes called (n+1/2) f_{ce} waves (Kazama et al., 2018; Kennel et al., 1970). LBC waves are electromagnetic and right-handed polarized waves excited in the lower frequency band of $0.5f_{ce}$. Electrons trapped by the Earth's magnetic field precipitate into the atmosphere when their trajectory is changed by plasma waves near the magnetic equator due to the violation of the first adiabatic invariant. The interaction between waves and electrons is particularly strong when the doppler-shifted wave frequency in the guiding center reference frame is nf_{ce}, where n is an integer. Electrons whose pitch angles become smaller than a loss-cone angle strike the atmosphere before bouncing back to the magnetosphere and consequently contribute to auroral emission. The typical cyclotron resonance energies of the ECH and LBC waves range from a few hundred to a few keV and from a few to tens of keV, respectively (e.g., Horne et al., 2003; Kurita et al., 2014; Miyoshi, Oyama, et al., 2015; Ni et al., 2008) .

In order to determine which plasma waves contribute to electrons scattering into the loss cone, it is essential to compare the plasma wave intensity and electron flux inside the loss cone with in-situ observations. (S. Kasahara et al., 2018) demonstrated one-to-one correspondence between the LBC wave intensity and 24.5 keV electron flux in the loss cone based on data obtained by the

Arase satellite. However, there is no observational evidence that ECH waves scatter electrons into the loss cone. In the outer magnetosphere where interaction with ECH waves leads to electron precipitation and diffuse auroral emissions, the loss-cone angle near the equatorial plane is too small compared to the inner magnetosphere, and therefore a spacecraft cannot measure the electron flux in the loss cone. In this study, we investigate whether ECH waves scatter electrons into the loss cone in the equatorial region of the inner magnetosphere by comparing electron fluxes in the loss cone with wave amplitudes and calculating pitch-angle diffusion coefficients.

2 Instrumentation

To measure electrons and plasma waves over a wide range of energies and frequencies, four particle experiments and Plasma-Wave Experiments (PWE) (Y. Kasahara et al., 2018), consisting of four subcomponents were conducted by the Arase satellite (Miyoshi, Shinohara, et al., 2018).

The low-energy particle experiment–electron analyzer (LEPe) measures electrons with energies from ~20 eV to ~20 keV (Kazama et al., 2017). To obtain the pitch-angle distribution, LEPe measures three-dimensional electron fluxes every spin (~8 s). There are two different types of channels: coarse channels for observing the electron's parallel and perpendicular temperature and pitch-angle distributions with a pitch-angle resolution of 22.5°, and fine channels for loss-cone measurements with a pitch-angle resolution of 3.75°. Only data from fine channels are used in this study.

The onboard frequency analyzer (OFA) (Matsuda et al., 2018), which is one of the PWE's receivers, obtains signals from two pairs of dipole wire-probe antennas (WPT) (Kasaba et al., 2017) and tri-axis magnetic search coils (Ozaki et al., 2018), and it produces a single-channel power spectrum for the electric and magnetic field (OFA-SPEC). The frequency range of OFA-SPEC is from 64 Hz to 20 kHz. During the time interval used in this study, the OFA provided 132-point frequency spectra with a time cadence of 1 s.

3 Data

During the period from 01:10 UT to 01:15 UT on April 15, 2017, in a substorm recovery phase, the Arase satellite was located in the post-midnight sector near the magnetic equator (L_m = 6.1 derived from IGRF, magnetic local time (MLT) = 3.2 h, and magnetic latitude (MLAT) = 0.0°–0.4°). Figures 1a and 1b show the wave power-spectral density of the electric and the magnetic field, respectively. The frequency has been normalized by f_{ce} in Figures 1a and 1b. We derived f_{ce} from the local ambient magnetic field measured by the magnetic field experiment (MGF) (Matsuoka et al., 2018). Quasi-periodic intense ECH emissions were observed in the first harmonic band (f_{ce}–$2f_{ce}$), while the amplitudes of the higher harmonic bands were small (Fig. 1a). Upper-band (> $0.5f_{ce}$) and lower-band (< $0.5f_{ce}$) chorus waves were observed throughout this period, and upper-band chorus waves appeared rather continuously (Fig. 1b).

Figures 1c and 1d show the electron energy flux in the field-aligned direction (with a pitch-angle range of 0°–3°) and outside a loss cone (with a pitch-angle range of 42°–45°), respectively. Although the electron flux outside the loss cone was relatively stable, the field-aligned electron flux had quasi-periodic modulations with a typical period of ~26 s. To visualize the differences between the electron flux inside and that outside the loss cone, we show the ratio of the electron fluxes (Fig. 1c, d, e).

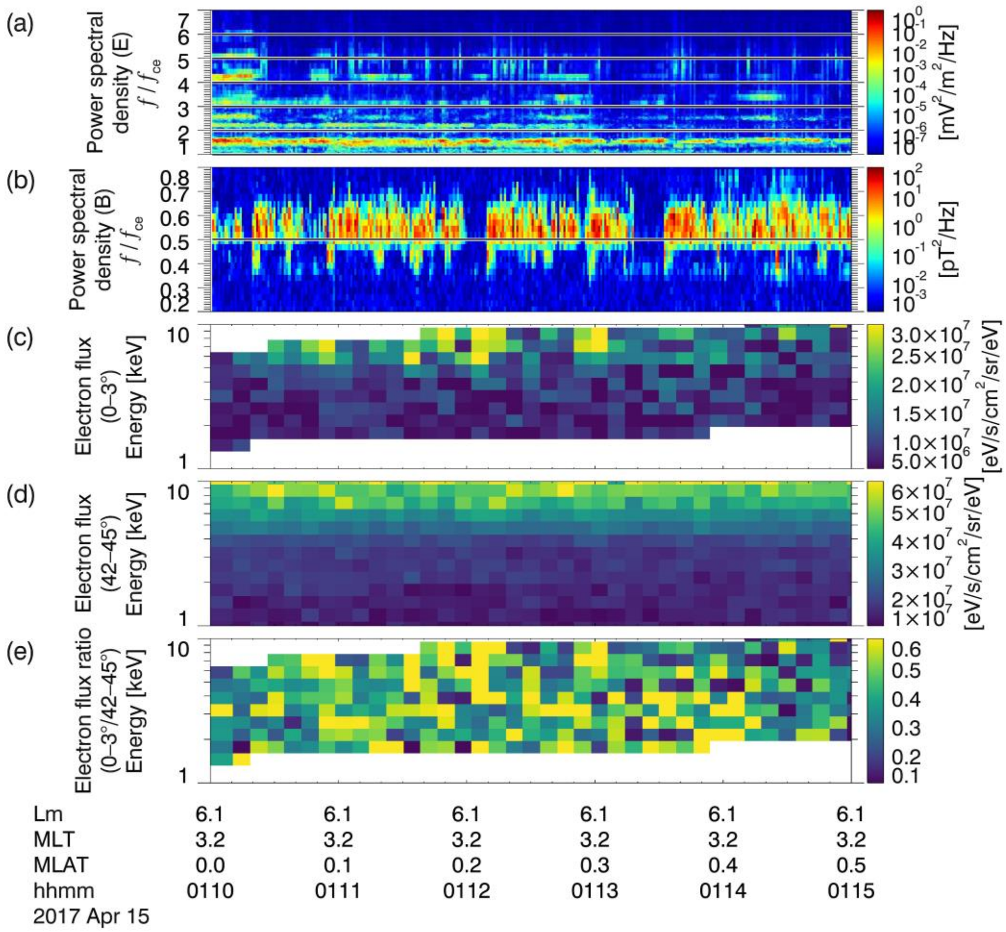

Figure 1 The wave power-spectral density of **(a)** the electric and **(b)** the magnetic field. The black solid lines indicate integer multiples of f_{ce} in (a) and $0.5f_{ce}$ in (b). Electron energy flux in the pitch-angle ranges of **(c)** 0°–3° and **(d)** 42°–45° observed by the fine channel of LEPe. **(e)** The ratio of (c) to (d) indicates the difference between the inside and the outside loss-cone electron flux.

It is difficult for Arase to observe an electron flux of specific energy in the loss cone continuously and for a long time because its direction relative to the ambient magnetic field changes. Therefore, we analyzed the available data as a 5-min event, as shown in Fig. 1.

4 Data Analysis and Results

To investigate the relationship between the waves and the electron flux inside the loss cone quantitatively, we calculate the cross-correlation coefficients between the temporal modulation of the wave intensity shown in Fig. 1a and 1b and the electron flux ratio shown in Fig. 1e. The ECH wave intensity is derived by integrating the wave power-spectral density based on the electric field measurements between f_{ce} and $2f_{ce}$ (Fig. 1a), and then converting it to mV/m. The LBC wave intensity is derived by integrating the wave power-spectral density obtained with the search coil magnetometer between $0.3f_{ce}$ and $0.5f_{ce}$ (Fig. 1b), and then converting it to nT. Before calculating the cross-correlation coefficients, we adjust the temporal resolution of the wave data (1 s) to that of the electron data (8 s). The downsampling procedure is as follows. We calculate the moving average of the wave data with a 9-s window, subtract the average, apply a Hanning window to perform a fast Fourier transform (FFT), removed the Nyquist effect by applying a low-pass filter with a cutoff frequency of 1/16 Hz, and perform an inverse FFT.

Figure 2a and 2b shows the temporal variability of the ECH and LBC wave intensities, respectively, converted to the 8-s values. The loss-cone flux ratio of the 4.8-keV electron, which is subtracted from the average flux ratio and on which we applied the Hanning window, is indicated with blue lines in Fig. 2a and 2b. The cross-correlation coefficients between them are 0.48 for ECH and −0.016 for LBC. Although the absolute value of the cross-correlation coefficient is not very high in the case of ECH, it is still large compared to the value for LBC and is statistically significant, as indicated by the obtained Student's t-test values. The estimated *p* value for ECH is $<3.5 \times 10^{-3}$, which is smaller than the significance level of 5.0×10^{-2}, whereas it is <1.0 for LBC. One of the causes of the reduction of the cross-correlation coefficient in the ECH case is that the loss-cone angle at the position of the Arase satellite is not always larger than the pitch-angle resolution of the fine LEPe channels. If we assume that the magnetic field strength in the ionosphere at the Arase footprint based on the magnetic field model TS04 (Tsyganenko & Sitnov, 2005) is 50,000 nT, the loss-cone angle at the Arase satellite is 2.4°, since the magnetic field strength at the position of the Arase satellite is 88 nT.

Figure 2c shows the cross-correlation coefficients of different energies against the wave intensity (red dots and solid line: ECH; blue dots and dashed line: LBC). The *p* value of the cross-correlation coefficient between the LBC wave and the loss-cone flux ratio of the 8.6-keV electron is 1.3×10^{-2}, which smaller than the significance level of 5.0×10^{-2}, whereas that for ECH is 1.5. These results reflect a positive correlation between the ECH wave intensity and the ~5 keV loss-cone energy flux, and between the LBC wave intensity and the ~9 keV loss-cone energy flux. This is consistent with the general characteristic of the typical resonance energy of LBC being larger than that of ECH.

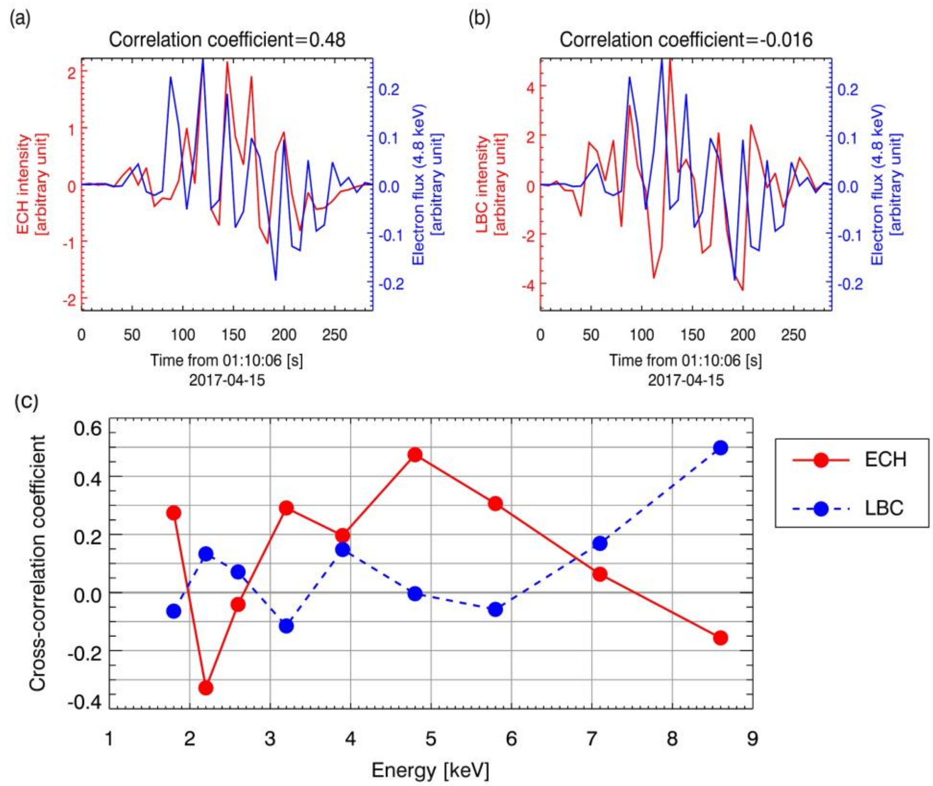

Figure 2 Temporal variability, from 01:10:06 UT, of **(a)** ECH and **(b)** LBC wave intensity is indicated with a red line, whereas the variability of the loss-cone flux ratio of the 4.8-keV electron is indicated with a blue line. The cross-correlation coefficient between the wave intensity and the electron influx is shown at the top of each panel. **(c)** The cross-correlation coefficients between the ECH wave intensity and the loss-cone electron flux ratio (shown with red dots and solid line, respectively), and those between the LBC wave intensity and the loss-cone electron flux ratio (shown with blue dots and dashed line, respectively) as a function of electron's energy.

5 Discussion

To calculate the resonance energy of ECH waves, the hot plasma dispersion relation must be solved. However, this cannot be easily done, as in the case of LBC. To quantitatively evaluate whether ECH waves can scatter 5 keV electrons into the loss cone, we calculate the pitch-angle diffusion coefficient of the ECH waves.

The pitch-angle diffusion coefficient for ECH waves was expressed by Horne & Thorne (2000) with the following equation

$$D_{\alpha\alpha} = \frac{\pi^{1/2}}{2}\frac{e^2}{m_{\mathrm{e}}^2}\frac{|\mathbf{E_w}|^2}{k_{\perp 0}^2 \Delta k_{\parallel}}\frac{1}{v^5\cos\alpha} \cdot \sum_{n=-\infty}^{\infty}\left(\frac{n\Omega_{\mathrm{e}} - \omega_{\mathbf{k}}\sin^2\alpha}{\sin\alpha\cos\alpha}\right)^2 \exp(-\lambda) I_n(\lambda) \cdot \{\exp[-(\zeta_n^-)^2] + \exp[-(\zeta_n^+)^2]\} \tag{1}$$

where $\zeta_n^{\pm} = (\omega_{\mathbf{k}} - n\Omega_{\mathrm{e}})/(\Delta k_{\parallel} v \cos\alpha) \pm k_{\parallel 0}/\Delta k_{\parallel}$, $\lambda = k_{\perp 0}^2 v_{\perp}^2/(2\Omega_{\mathrm{e}}^2)$; $k_{\perp 0}$ and $k_{\parallel 0}$ are the components of the resonant wavenumber vector perpendicular and parallel to the ambient magnetic field $\mathbf{B}_0$, respectively; $\Delta k_{\parallel}$ is the width of the spectrum; $\Omega_{\mathrm{e}} = 2\pi f_{\mathrm{ce}} = |e\mathbf{B_0}/m_{\mathrm{e}}|$ is the angular electron cyclotron frequency; $\omega_{\mathbf{k}}$ is the wave frequency as a function of $\mathbf{k}$; $|\mathbf{E_w}|$ is the wave electric field; α and v are the particle pitch angle and velocity, respectively; e/m_{e} is the electron charge to mass ratio; and I_{n} is the modified Bessel function of order n. Horne & Thorne (2000) neglected the parallel group velocity, because it is small compared to the electron parallel velocity. In addition, they approximated $k^2 = k_{\perp}^2$, where $k_{\perp}$ is the wavenumber *k*, which is perpendicular to the ambient magnetic field, since the ECH waves propagate at large angles with respect to the magnetic field. Assuming that the local diffusion coefficient remains approximately constant within this narrow MLAT range from −3° to 3°, where ECH waves are typically excited (Gough et al., 1979; Meredith et al., 2009), and neglecting any variations due to changes in the pitch angle, the bounce-averaged diffusion coefficient can be approximated as (Horne & Thorne, 2000)

$$\begin{aligned} \langle D_{\alpha\alpha} \rangle &\approx \frac{D_{\alpha\alpha}}{T_{\mathrm{b}}} \int_{-\lambda_{\mathrm{int}}}^{\lambda_{\mathrm{int}}} \frac{2}{v \cos\alpha_{\mathrm{eq}}} ds \\ &= T_{\mathrm{frac}} D_{\alpha\alpha} \end{aligned} \tag{2}$$

where $T_{\mathrm{frac}} = 4LR_{\mathrm{e}}\lambda_{\mathrm{int}}/v\cos\alpha_{\mathrm{eq}}\, T_{\mathrm{b}}$ is the fraction of time when the particle interacts with the wave during one bounce period, T_{b} is the particle bounce period, α_{eq} is the pitch angle at the magnetic equator, λ_{int} is the upper limit of integration in MLAT, and R_{e} is Earth's radius. We set $T_{\mathrm{frac}} = 1$ for electrons with a mirror point smaller than λ_{int}.

The input parameters were $|\mathbf{E_w}| = 1.0$ mV/m, $\omega_{\mathbf{k}} = 1.6\Omega_{\mathrm{e}}$, and $f_{\mathrm{ce}} = \Omega_{\mathrm{e}}/(2\pi) = 2.5$ kHz, based on OFA and MGF observation data, as shown in Fig. 1a. We also set other parameters as $L = 6.1$, $\lambda_{\mathrm{int}} = 3.0°$, and $\alpha = 0$– $3°$. To determine the parameters $k_{\perp 0}$, $k_{\parallel 0}$, and $\Delta k_{\parallel 0} = k_{\perp 0}/\tan(\psi - \Delta\psi) - k_{\parallel 0}$, we need to know *k* and the wave normal angle ψ, which cannot be obtained from the Arase observations, because PWE measures only two components of the electric field. Changing the wave normal angle to the background magnetic field from 85.0° to 89.5°, Kyoto University Plasma Dispersion Analysis Package (KUPDAP, Sugiyama et al., 2015) was used to obtain the k, which corresponds to $\omega_{\mathbf{k}} = 1.6\Omega_{\mathrm{e}}$. The input parameters for KUPDAP, i.e., the electron temperature, the electron density, and the loss-cone depth and width, were determined by fitting the phase space density recorded on the fine LEPe channel with a sum of five subtracted Maxwellian components, as shown in Fig. 3 and Table 1, in agreement with previous studies (Ashour-Abdalla & Kennel, 1978; Horne et al., 2003; Liang et al., 2010). The input parameters of the coldest component (component 1 in Table 1) cannot be obtained from the Arase observation since the lower-limit energy of LEPe is about 20 eV. It is difficult to precisely determine the cold electron density from the UHR frequency, because the UHR wave was not detectable during our interested period. However, we estimate the cold electron density using the electrostatic (n+1/2) f_{ce} emissions as a diagnostic tool (Hubbard et al., 1979). Hubbard et al. (1979) found that the maximum value of *n* depends of the combination on the ratios of cold (<10 eV) to hot plasma density $n_{\mathrm{c}}/n_{\mathrm{h}}$, and of the plasma frequency to the cyclotron frequency $f_{\mathrm{p}}/f_{\mathrm{ce}}$. During most of the time shown in Fig. 1a, electrostatic emissions are excited up to (5+1/2) f_{ce}. If we assume that the hot electron density is the sum of electron densities of components 2–4 in Table 1, then the estimated cold electron density is 1.9/cm^3. We also assume that the electron

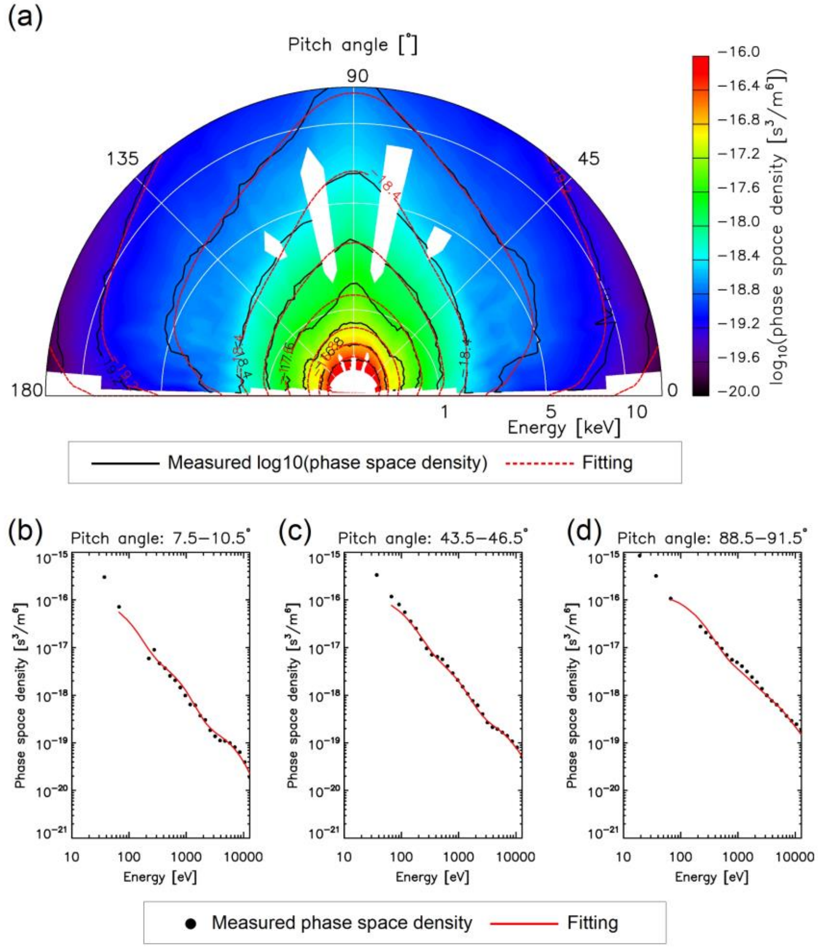

Figure 3 (a) Electron pitch-angle distribution recorded on the fine LEPe channel (filled contour and black solid lines). The phase space density is averaged over a period of 3 minutes from 01:10–01:13 UT. The contour of the modeled distribution is indicated with dashed red lines. Measured (dots) and modeled (red solid line) electron distribution functions at the pitch angles of (b) 7.5°–10.5°, (c) 43.5°–46.5°, and (d) 88.5°–91.5° in (a).

temperature of the coldest component ranges from 1 eV to 10 eV. To maintain the quasineutrality, the proton's distribution function is assumed to be the Maxwellian, whose temperature and density are 1 eV and 2.8/cm^3, respectively.

We calculate the bounce-averaged pitch-angle diffusion coefficients near the loss cone as a function of electron energy by changing wave normal angle of the ECH waves and temperature of coldest electrons. From Fig. 2c, it is expected that the pitch-angle diffusion coefficient of the ECH wave has a peak at 5 keV. Among the combinations of the electron temperature and the wave normal angle that peak at the pitch-angle diffusion coefficient of 5 keV, the linear growth rate of the first harmonic band of the ECH wave calculated using KUPDAP is largest at 8 eV and 88.5°. Under these conditions, it is reasonable that the ECH wave contributes to scattering of electrons for 5 keV.

Table 1 Parameters of multicomponent subtracted Maxwellian in Equation (1) of Liang et al. (2010). The parameters of coldest component 1 are not the result of fitting but of assumption.

Component	$T_\perp$ [eV]	$T_{\parallel}$ [eV]	n [cm^{-3}]	Δ	β
1	1–10	1–10	1.9	1.0	0.0
2	130	57	0.18	0.90	0.015
3	630	440	0.16	0.82	0.019
4	3.1×10^{3}	350	0.12	0.73	0.010
5	3.7×10^{3}	4.2×10^{3}	0.072	0.63	2.0×10^{-3}
6	1.8×10^{4}	5.0×10^{3}	0.33	0.20	0.016

The calculated parallel cyclotron resonance energy of LBC at this time is 4 keV, based on the first-order cyclotron resonance condition in Kennel & Petschek (1966). The cyclotron resonance energy of the LBC near the magnetic equator is smaller than the energy that correlates with the loss-cone flux. However, the LBC waves grow and their resonance energies also increase as they propagate to the higher MLAT (Miyoshi et al., 2010; Miyoshi, Oyama, et al., 2015), causing pitch-angle scattering of ~9 keV electrons. The resonance energy of LBC reaches 9 keV at the MLAT of −3° in this event.

Unfortunately, we cannot confirm whether auroral emissions are caused by the electron precipitation, because the footprint of the Arase satellite is in the sunlit region. We estimated the column emission intensity of oxygen 557.7 nm aurora at about 200 R based on the electron flux measured by Arase, which is correlated with the ECH wave intensity. The auroral intensity is estimated using the electron two-stream model (Ono, 1993). The IRI and MSIS models are used to evaluate ionosphere and thermosphere conditions at the footprint of Arase. To estimate the auroral intensity, the downward electron energy flux F at the ionospheric altitudes is estimated as $F \approx \left(B_{\mathrm{i}}/B_{\mathrm{eq}}\right)EJ_{\mathrm{eq}}\Delta\Omega\Delta E$ (S. Kasahara et al., 2018), where B_i and B_{eq} are the magnetic field strength at the ionosphere and at the equator, respectively; E is the electron's characteristic energy; J_{eq} is the differential number flux at the magnetic equator; $\Delta\Omega$ is the solid angle of the loss cone; and ΔE is the energy range of precipitation electrons. We adopt $E \approx 5$ keV and $\Delta E \approx 2$ keV from Fig. 2(c), take $B_i \approx 50{,}000$ nT, $B_{\mathrm{eq}} \approx 88$ nT, $J_{\mathrm{eq}} \approx 4.6 \times 10^{6}$/s/sr/cm^2/keV, and $\Delta\Omega \approx 3.7 \times 10^{-3}$ sr, and adopt a downward electron energy flux of approximately 9.7×10^{7} keV/cm^2/s, or 0.15 erg/cm^2/s, which contributes to the visible auroral emissions.

6 Summary

In this study, we compared the ECH wave intensity with the electron flux in the loss cone for the first time. To investigate quantitatively whether ECH waves cause the pitch-angle scattering of electrons in the inner magnetosphere, we calculated the cross-correlation coefficient between the ECH wave intensity and the electron flux in the loss cone observed by the Arase satellite. We found an event during which the ~5 keV electron loss-cone flux is correlated with the ECH wave intensity. The pitch-angle diffusion coefficient was calculated in order to evaluate whether the observed ECH wave could scatter 5 keV electrons into the loss cone. The pitch-angle diffusion

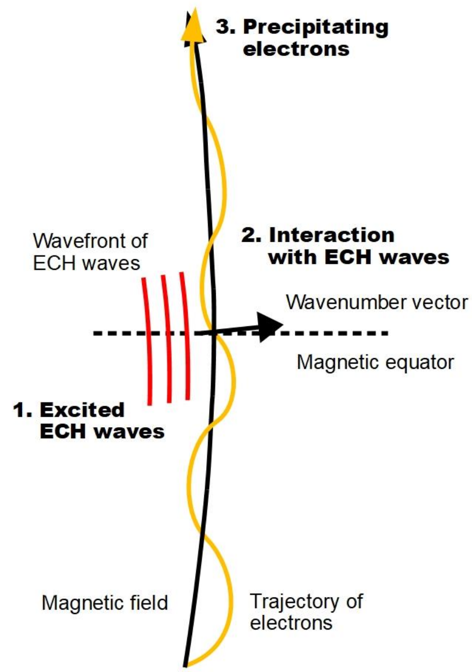

Figure 4 Schematic diagram showing that ECH waves excited in the magnetic equator propagate in the direction nearly perpendicular to the ambient magnetic field and scatter electrons into a loss cone, causing electron precipitation into the Earth's atmosphere, which contributes to auroral emission.

coefficient for 5 keV electrons is relatively larger than that for other energy electrons when the electron temperature is 8 eV and the wave normal angle is 88.5°. The observed electron flux correlated with the ECH wave can cause 557.7 nm auroral emission with brightness of about 200 R. These results suggest that ECH waves propagating nearly perpendicular to the ambient magnetic field scatter a few keV electrons into a loss cone near the magnetic equator of the inner magnetosphere, and probably produce diffuse or pulsating auroral emission, as illustrated in Fig. 4. Since this study concerns an event study, statistical analysis is further required.

Acknowledgments

Science data of the ERG (Arase) satellite were obtained from the ERG Science Center operated by ISAS/JAXA and ISEE/Nagoya University (https://ergsc.isee.nagoya-u.ac.jp/index.shtml.en, Miyoshi, Hori, et al., 2018). The present study analyzed MGF-L2 v03_03 data and PWE/OFA-L2 v02_01 data. The SPEDAS software (Angelopoulos et al., 2019) was used for the data analysis in this study. LEPe data are based on L1 version 6 (calibrated, equivalent to L2 v02_02) and MGF-L2 v03_03. The LEPe data will be publicly available when this paper is published. The development and operation of LEPe is partly funded by Academia Sinica and National Cheng Kung University of Taiwan and also through the support of Ministry of Science and Technology of Taiwan under contract 106-2111-M-001-011 and 105-3111-Y-001-042. The first author is a Research Fellow of Japan Society for the Promotion of Science (DC). This study is supported by JSPS Bilateral Open Partnership Joint Research Projects, JSPS KAKENHI Grant Numbers JP15H05815, JP18H03727, JP20H01959, and JP20J11829 and carried out by the joint research program of the Institute for Space-Earth Environmental Research (ISEE), Nagoya University.

References

Angelopoulos, V., Cruce, P., Drozdov, A., Grimes, E. W., Hatzigeorgiu, N., King, D. A., et al. (2019). *(SPEDAS). Space Sci Rev*. The Author(s). https://doi.org/10.1007/s11214-018-0576-4

Ashour-Abdalla, M., & Kennel, C. F. (1978). Nonconvective and Convective Electron Cyclotron Harmonic Instability. *Journal of Geophysical Research*, *83*(1531). https://doi.org/10.1029/JA083iA04p01531

Fukizawa, M., Sakanoi, T., Miyoshi, Y., Hosokawa, K., Shiokawa, K., & Katoh, Y. (2018). Electrostatic Electron Cyclotron Harmonic Waves as a Candidate to Cause Pulsating Auroras. *Geophysical Research Letters*, *45*(12), 661–668. https://doi.org/10.1029/2018GL080145

Gough, M. P., CHristiansen, P. J., Martelli, G., & Gershuny, E. J. (1979). Interaction of electrostatic waves with warm electrons at the geomagnetic equator. *Nature*, *279*(5713), 515–517. https://doi.org/10.1038/279515a0

Horne, R. B., & Thorne, R. M. (2000). Electron pitch angle diffusion by electrostatic electron cyclotron harmonic waves: The origin of pancake distributions. *Journal of Geophysical Research*, *105*, 5391–5402. https://doi.org/10.1029/1999JA900447

Horne, R. B., Thorne, R. M., Meredith, N. P., & Anderson, R. R. (2003). Diffuse auroral electron scattering by electron cyclotron harmonic and whistler mode waves during an isolated substorm. *Journal of Geophysical Research: Space Physics*, *108*(A7), 1–12. https://doi.org/10.1029/2002JA009736

Hosokawa, K., Miyoshi, Y., Ozaki, M., Oyama, S., Ogawa, Y., Kurita, S., et al. (2020). Multiple time-scale beats in aurora : precise orchestration via magnetospheric chorus waves. *Scientific Reports*, 1–10. https://doi.org/10.1038/s41598-020-59642-8

Hubbard, R. F., Birmingham, T. J., & Hones, E. W. (1979). Magnetospheric electrostatic emissions and cold plasma densities. *Journal of Geophysical Research*, *84*, 5828–5838. https://doi.org/10.1029/JA084iA10p05828

Kasaba, Y., Ishisaka, K., Kasahara, Y., Imachi, T., Yagitani, S., Kojima, H., et al. (2017). Wire Probe Antenna (WPT) and Electric Field Detector (EFD) of Plasma Wave Experiment (PWE) aboard the Arase satellite: specifications and initial evaluation results. *Earth, Planets and Space*, *69*(1). https://doi.org/10.1186/s40623-017-0760-x

Kasahara, S., Miyoshi, Y., Yokota, S., Mitani, T., Kasahara, Y., Matsuda, S., et al. (2018). Pulsating aurora from electron scattering by chorus waves. *Nature*, *554*(7692), 337–340. https://doi.org/10.1038/nature25505

Kasahara, Y., Kasaba, Y., Kojima, H., Yagitani, S., Ishisaka, K., Kumamoto, A., et al. (2018). The Plasma Wave Experiment (PWE) on board the Arase (ERG) satellite. *Earth, Planets and Space*, *70*(1). https://doi.org/10.1186/s40623-018-0842-4

Kazama, Y., Wang, B. J., Wang, S. Y., Ho, P. T. P., Tam, S. W. Y., Chang, T. F., et al. (2017). Low-energy particle experiments–electron analyzer (LEPe) onboard the Arase spacecraft. *Earth, Planets and Space*, *69*(1). https://doi.org/10.1186/s40623-017-0748-6

Kazama, Y., Kojima, H., Miyoshi, Y., Kasahara, Y., Usui, H., Wang, B., et al. (2018). Density Depletions Associated With Enhancements of Electron Cyclotron Harmonic Emissions : An ERG Observation Special Section : *Geophysical Research Letters*, 75–83. https://doi.org/10.1029/2018GL080117

Kennel, C. F., & Petschek, H. E. (1966). Limit on stably trapped particle fluxes. *Journal of Geophysical Research*, *71*(1), 1–28. https://doi.org/10.1029/JZ071i001p00001

Kennel, C. F., Scarf, F. L., Fredricks, R. W., McGehee, J. H., & Coroniti, F. V. (1970). VLF electric field observations in the magnetosphere. *Journal of Geophysical Research*, *75*(31), 6136–6152. https://doi.org/10.1029/JA075i031p06136

Kurita, S., Miyoshi, Y., Cully, C. M., Angelopoulos, V., Contel, O. Le, Hikishima, M., & Misawa, H. (2014). Observational evidence of electron pitch angle scattering driven by ECH waves. *Geophysical Research Letters*, *41*(22), 8076–8080. https://doi.org/10.1002/2014GL061927

Liang, J., Uritsky, V., Donovan, E., Ni, B., Spanswick, E., Trondsen, T., et al. (2010). THEMIS observations of electron cyclotron harmonic emissions, ULF waves, and pulsating auroras. *Journal of Geophysical Research: Space Physics*, *115*(10), 1–24. https://doi.org/10.1029/2009JA015148

Lyons, R. (1974). Electron diffusion driven by magnet ospheric electrostatic waves. *Journal of Geophysical Research*, *79*(4), 575–580. https://doi.org/https://doi.org/10.1029/JA079i004p00575

Matsuda, S., Kasahara, Y., Kojima, H., Kasaba, Y., Yagitani, S., Ozaki, M., et al. (2018). Onboard software of Plasma Wave Experiment aboard Arase: instrument management and signal processing of Waveform Capture/Onboard Frequency Analyzer. *Earth, Planets and Space*, *70*(1). https://doi.org/10.1186/s40623-018-0838-0

Matsuoka, A., Teramoto, M., Nomura, R., Nosé, M., Fujimoto, A., Tanaka, Y., et al. (2018). The ARASE (ERG) magnetic field investigation. *Earth, Planets and Space*, *70*(1), 1–16. https://doi.org/10.1186/s40623-018-0800-1

Meredith, N. P., Horne, R. B., Thorne, R. M., & Anderson, R. R. (2009). Survey of upper band chorus and ECH waves: Implications for the diffuse aurora. *Journal of Geophysical Research: Space Physics*, *114*(7), 1–11. https://doi.org/10.1029/2009JA014230

Miyoshi, Y., Katoh, Y., Nishiyama, T., Sakanoi, T., Asamura, K., & Hirahara, M. (2010). Time of flight analysis of pulsating aurora electrons, considering wave-particle interactions with propagating whistler mode waves. *Journal of Geophysical Research: Space Physics*, *115*(10), 1–7. https://doi.org/10.1029/2009JA015127

Miyoshi, Y., Oyama, S., Saito, S., Kurita, S., Fujiwara, H., Kataoka, R., et al. (2015). Energetic electron precipitation associated with pulsating aurora: EISCAT and Van Allen Probe observations. *Journal of Geophysical Research : Space Physics*, *120*, 2754–2766. https://doi.org/10.1002/2014JA020690.Received

Miyoshi, Y., Saito, S., Seki, K., Nishiyama, T., Kataoka, R., Asamura, K., et al. (2015). Relation between energy spectra of pulsating aurora electrons and frequency spectra of whistler-mode chorus waves. *Journal of Geophysical Research: Space Physics*, 1–9. https://doi.org/10.1002/2015JA021562.Received

Miyoshi, Y., Shinohara, I., Takashima, T., Asamura, K., Higashio, N., Mitani, T., et al. (2018). Geospace exploration project ERG. *Earth, Planets and Space*, *70*(1), 101. https://doi.org/10.1186/s40623-018-0862-0

Miyoshi, Y., Hori, T., Shoji, M., Teramoto, M., Chang, T. F., Segawa, T., et al. (2018). The ERG Science Center. *Earth, Planets and Space*, *70*(1). https://doi.org/10.1186/s40623-018-0867-8

Ni, B., Thorne, R. M., Shprits, Y. Y., & Bortnik, J. (2008). Resonant scattering of plasma sheet electrons by whistler-mode chorus: Contribution to diffuse auroral precipitation. *Geophysical Research Letters*, *35*(11), 1–5. https://doi.org/10.1029/2008GL034032

Ono, T. (1993). Derivation of Energy Parameters of Precipitating Auroral Electrons by Using the Intensity Ratios of Auroral Emissions. *Journal of Geomagnetism and Geoelectricity*, *45*(6), 455–472. https://doi.org/https://doi.org/10.5636/jgg.45.455

Ozaki, M., Yagitani, S., Kasahara, Y., Kojima, H., Kasaba, Y., Kumamoto, A., et al. (2018). Magnetic Search Coil (MSC) of Plasma Wave Experiment (PWE) aboard the Arase (ERG) satellite. *Earth, Planets and Space*, *70*(1), 1–13. https://doi.org/10.1186/s40623-018-0837-1

Sugiyama, H., Singh, S., Omura, Y., Shoji, M., Nunn, D., & Summers, D. (2015). Electromagnetic ion cyclotron waves in the Earth's magnetosphere with a kappa-Maxwellian particle distribution. *Journal of Geophysical Research A: Space Physics*, *120*(10), 8426–8439. https://doi.org/10.1002/2015JA021346

Tsyganenko, N. A., & Sitnov, M. I. (2005). Modeling the dynamics of the inner magnetosphere during strong geomagnetic storms. *Journal of Geophysical Research: Space Physics*, *110*(A3), 1–16. https://doi.org/10.1029/2004JA010798